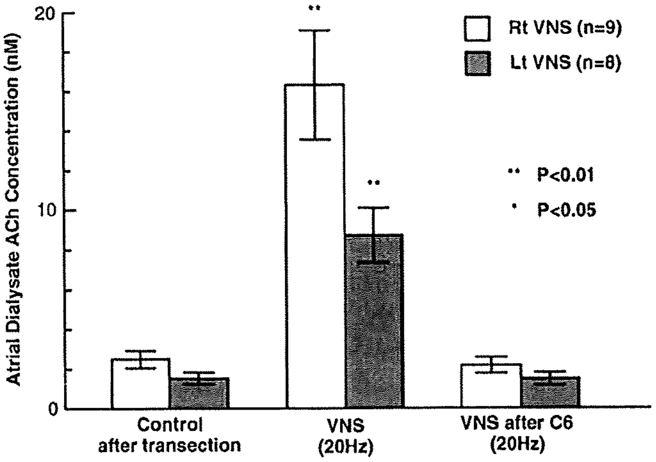

Fig. 4. Influence of ganglionic blocker on vagal nerve stimulation-induced ACh release. Right vagal nerve stimulation significantly increased atrial dialysate ACh concentration from 2.5 ± 0.4 to 16.3 ± 2.8 ($P<0.01$), and intravenous administration of hexamethonium suppressed the ACh concentration to 2.2 ± 0.4 nM. Left vagal stimulation increased atrial dialysate ACh concentration from 1.5 ± 0.3 to 8.7 ± 1.4 nM ($P<0.01$), and hexamethonium suppressed the ACh concentration to 1.5 ± 0.3 nM. Values are means ± SE; Rt: right; Lt: left; VNS: electrical vagal nerve stimulation; C6: hexamethonium bromide; *n*: number of rabbits; $^{**}P<0.01$ vs. control; $^{*}P<0.05$ vs. control.

cervical vagal stimulation decreased the atrial rates to 16.3% and 48.7%, respectively, of prestimulation rates in dogs. In our study, right and left vagal stimulation at a frequency of 40 Hz also decreased the atrial rate to 30% and 42% of prestimulation rates. The difference in atrial rate response between right and left vagal nerve stimulation could be explained by the different innervation densities of the right and left vagal nerves in the right atrium including the SA node. The SA node is innervated by both right and left vagal nerves with a predominance of right vagal nerves (Ardell and Randall, 1986; Randall et al., 1985), and the response of atrial rate to vagal nerve stimulation could be ascribed to vagal ACh release into the SA node. The SA node is probably regulated by ACh released from the left as well as the right vagal nerves. In this study, dialysate ACh concentration in the right atrium (logarithmically transformed) correlated well with atrial rate, and this correlation was independent of right or left vagal stimulation (Fig. 2). These results suggest that dialysate ACh in the right atrium reflects ACh released into the SA node independent of whether the ACh originates from the right or left vagal nerves.

4.2. ACh release in atrium and ventricle

In this study, the mean dialysate ACh concentration in the right ventricle after transection of bilateral vagal nerves was 20 to 30% of that in the right atrium. During vagal nerve stimulation at 20 Hz, the atrial dialysate ACh concentration increased 5 to 7 times the control value but the ventricular dialysate ACh concentration increased to only 2 to 3 times the control value (Fig. 3). This difference between atrial and ventricular dialysate ACh concentrations could be related to the density of vagal innervation. These results are consistent with previous *in vitro* studies (Kilbinger and Löffelholz, 1976; Brown, 1976; Stanley et al., 1978). Kent et al. (1974) reported that the atrial myocardium of the vertebrate heart was richly innervated as identified by specific histochemical staining of acetylcholinesterase, in contrast to the scant innervation in the ventricular myocardium.

Right vagal nerve stimulation increased atrial dialysate ACh more than left stimulation. On the other hand, there was no difference in ventricular dialysate ACh concentration between right and left vagal nerve stimulation. Although the right atrium is predominantly innervated by the right vagal nerves, the right ventricle could be equally innervated by the right and left vagal nerves. When the right vagal nerve was stimulated at 20 Hz, heart rate decreased from 305 ± 3 to 122 ± 4 bpm. When the left vagal nerve was stimulated at 20 Hz, heart rate decreased from 306 ± 5 to 169 ± 19 bpm. This difference in heart rate response could be ascribed to vagal ACh release into the SA node. Atrial dialysate ACh concentrations were 17.9 ± 4.0 and 7.9 ± 1.4 nM ($P<0.05$) during stimulation of right and left vagal nerves, respectively. In contrast, there was no significant difference in ventricular dialysate ACh concentration between right and left vagal nerve stimulation. Therefore, we consider that dialysate ACh concentration in the right atrium may be a better index of ACh release into the SA node than dialysate ACh in the right ventricle.

4.3. Source of atrial dialysate ACh

In a previous study with anesthetized cats, we demonstrated that ACh in the dialysate sampled from left ventricular myocardium primarily reflects ACh released from postganglionic cardiac vagal nerves (Akiyama et al., 1994). Cardiac ganglia are located predominantly in the posterior aspect of the atria within the subepicardial connective tissue (Löffelholz and Pappano, 1985). It is possible that ACh released from stimulated preganglionic nerves contributes to ACh in the dialysate sampled from the right atrium. In this study, intravenous administration of hexamethonium bromide, a nicotinic antagonist, abolished the increase in ACh release during efferent vagal nerve stimulation. This result demonstrates that ACh in the dialysate sampled from the right atrium primarily originates from the postganglionic cardiac nerve endings.

4.4. Significance of monitoring ACh release to the SA node

Several studies have directly measured electrical efferent vagal nerve activities at the preganglionic site in vivo (Jewett, 1964; Kunze, 1972). Although this method has been used to estimate the net activity of cardiac vagal nerves, it is technically difficult to selectively measure the electrical activity of postganglionic vagal nerves innervating the SA node. Moreover, it is possible that preganglionic signals are modulated at intracardiac ganglionic sites (Gray et al., 2004). In fact, Bibevski and Dunlap (1999) have reported that attenuated vagal control in heart failure can be ascribed to attenuated ganglionic transmission. Therefore, information about postganglionic vagal nerve activity is important for understanding vagal control of heart rate.

4.5. Methodological consideration

First, we sectioned the vagi in the neck region but the sympathetic nerves were almost intact because the sympathetic nerves run separately from the vagi at the neck in rabbits. ACh released from vagal nerve terminals may interact with muscarinic receptors on postganglionic sympathetic nerve terminals to inhibit norepinephrine release prejunctionally (Levy, 1984).

Second, ACh is degraded by ACh esterase immediately after its release. Therefore to detect ACh release in vivo, addition of a specific ACh esterase inhibitor eserine into the perfusate is necessary. We used eserine at a concentration 10–100 times higher than that required in *in vitro* experimental settings because distribution of eserine across the semipermeable membrane is required, based on previous results (Akiyama et al., 1994). Eserine should spread around the semipermeable membrane, thereby affecting the ACh release in the vicinity of the dialysis membrane. Eserine may have increased the ACh level in the synaptic cleft and enhanced heart rate response by nerve stimulation, and may have also activated regulatory pathways such as autoinhibition of ACh release via muscarinic receptors.

5. Conclusion

We were able to monitor myocardial interstitial ACh levels in the right atrium around the SA node using a microdialysis technique.

Myocardial interstitial ACh level in the right atrium correlates well with atrial rate. Microdialysis combined with HPLC will become a powerful tool for understanding the parasympathetic control of heart rate.

Acknowledgements

This study was supported by Grants-in-Aid for scientific research (No. 19591829 and 20390462) from the Ministry of Education, Culture, Sports, Science and Technology; by Health and Labor Sciences Research Grants (H18-Iryo-Ippan-023, H18-nano-Ippan-003, H19-nano-Ippan-009 and H20-katsudo-Shitei-007) from the Ministry of Health, Labour and Welfare of Japan; and by the Industrial Technology Research Grant Program from New Energy and Industrial Technology Development Organization of Japan.

References

Akiyama, T., Yamazaki, T., Ninomiya, I., 1994. In vivo detection of endogenous acetylcholine release in cat ventricles. Am. J. Physiol. 266, H854–860.

Ardell, J.L., Randall, W.C., 1986. Selective vagal innervation of sinoatrial and atrioventricular nodes in canine heart. Am. J. Physiol. 251, H764–773.

Bibevski, S., Dunlap, M.E., 1999. Ganglionic mechanisms contribute to diminished vagal control in heart failure. Circulation 99, 2958–2963.

Brown, O.M., 1976. Cat heart acetylcholine: structural proof and distribution. Am. J. Physiol. 231, 781–785.

Glantz, S.A., 2005. Primer of Biostatistics, 6th ed. McGraw-Hill, New York.

Gray, A.L., Johnson, T.A., Ardell, J.L., Massari, V.J., 2004. Parasympathetic control of the heart. II. A novel interganglionic intrinsic cardiac circuit mediates neural control of heart rate. J. Appl. Physiol. 96, 2273–2278.

Jewett, D.L., 1964. Activity of single efferent fibres in the cervical vagus nerve of the dog, with special reference to possible cardio-inhibitory fibres. J. Physiol. 175, 321–357.

Kawada, T., Yamazaki, T., Akiyama, T., Shishido, T., Inagaki, M., Uemura, K., Miyamoto, T., Sugimachi, M., Takaki, H., Sunagawa, K., 2001. In vivo assessment of acetylcholine-releasing function at cardiac vagal nerve terminals. Am. J. Physiol. Heart Circ. Physiol. 281, H139–145.

Kent, K.M., Epstein, S.E., Cooper, T., Jacobowitz, D.M., 1974. Cholinergic innervation of the canine and human ventricular conducting system. Anatomic and electrophysiologic correlations. Circulation. 50, 948–955.

Kilbinger, H., Löffelholz, K., 1976. The isolated perfused chicken heart as a tool for studying acetylcholine output in the absence of cholinesterase inhibition. J. Neural Transm. 38, 9–14.

Kunze, D.L., 1972. Reflex discharge patterns of cardiac vagal efferent fibres. J. Physiol. 222, 1–15.

Levy, M.N., 1984. Cardiac sympathetic–parasympathetic interactions. Fed. Proc. 43, 2598–2602.

Löffelholz, K., Pappano, A.J., 1985. The parasympathetic neuroeffector junction of the heart. Pharmacol. Rev. 37, 1–24.

Randall, W.C., Ardell, J.L., Becker, D.M., 1985. Differential responses accompanying sequential stimulation and ablation of vagal branches to dog heart. Am. J. Physiol. 249, H133–140.

Stanley, R.L., Conaster, J., Dettbarn, W.D., 1978. Acetylcholine, choline acetyltransferase and cholinesterases in the rat heart. Biochem. Pharmacol. 27, 2409–2411.

Autonomic Neuroscience: Basic and Clinical 152 (2010) 115–118

Contents lists available at ScienceDirect

Autonomic Neuroscience: Basic and Clinical

journal homepage: www.elsevier.com/locate/autneu

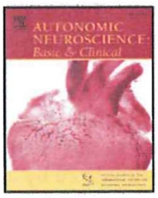

Short communication

In vivo direct monitoring of interstitial norepinephrine levels at the sinoatrial node

Shuji Shimizu [a,c,d,*], Tsuyoshi Akiyama [b], Toru Kawada [a], Toshiaki Shishido [a], Masaki Mizuno [a], Atsunori Kamiya [a], Toji Yamazaki [b], Shunji Sano [c], Masaru Sugimachi [a]

[a] Department of Cardiovascular Dynamics, Advanced Medical Engineering Center, National Cardiovascular Center Research Institute, Osaka, Japan
[b] Department of Cardiac Physiology, National Cardiovascular Center Research Institute, Osaka, Japan
[c] Department of Cardiovascular Surgery, Okayama University Graduate School of Medicine, Dentistry and Pharmaceutical Sciences, Okayama, Japan
[d] Japan Association for the Advancement of Medical Equipment, Tokyo, Japan

ARTICLE INFO

Article history:
Received 1 June 2009
Received in revised form 12 August 2009
Accepted 27 August 2009

Keywords:
Heart rate
Sympathetic nerve terminal activity
Norepinephrine
Sinoatrial node
Microdialysis
Desipramine

ABSTRACT

We assessed in vivo interstitial norepinephrine (NE) levels at the sinoatrial node in rabbits, using microdialysis technique. A dialysis probe was implanted adjacent to the sinoatrial node of an anesthetized rabbit and dialysate was sampled during sympathetic nerve stimulation. Atrial dialysate NE concentration correlated well with heart rate. Desipramine significantly increased dialysate NE concentrations both before and during sympathetic nerve stimulation compared with the absence of desipramine. However, desipramine did not affect the relation between heart rate and dialysate NE concentration. These results suggest that atrial dialysate NE level reflects the relative change of NE concentration in the synaptic cleft. Microdialysis is a powerful tool to assess in vivo interstitial NE levels at the sinoatrial node.

1. Introduction

Heart rate is determined by the frequency of depolarization of sinoatrial (SA) nodal cell during sinus rhythm. The SA node is innervated by sympathetic nerve fibers. These sympathetic nerves, together with parasympathetic nerves, play an important role in the regulation of SA node pacemaker activities. Direct measurement of electrical axonal activity of efferent cardiac sympathetic nerve (Kawada et al., 2004) and indirect measurement of norepinephrine (NE) spillover from plasma NE concentration in the coronary sinus (Meredith et al., 1993) have been used as indices of sympathetic nerve terminal activity on the effector, i.e. sinoatrial node. However, due to the heterogeneity of sympathetic innervation in the heart, quantitative assessment of sympathetic nerve terminal activities on the SA node is essential for better understanding of the sympathetic control of heart rate.

Recently we have developed a microdialysis technique that allows direct monitoring of acetylcholine release into the SA node (Shimizu et al., 2009). In the present study, we monitored interstitial NE levels in the right atrial myocardium adjacent to the SA node using the microdialysis technique and investigated the relation between interstitial NE levels and heart rate in response to sympathetic nerve stimulation. This study may prove the usefulness of microdialysis in assessing the relative change of sympathetic nerve terminal activity on the SA mode.

2. Materials and methods

2.1. Surgical preparation

Animal care was provided in accordance with the *Guiding Principles for the Care and Use of Animals in the Field of Physiological Sciences* approved by the Physiological Society of Japan. All protocols were approved by the Animal Subject Committee of the National Cardiovascular Center. Fourteen Japanese white rabbits weighing 2.4 to 2.8 kg were used in this study. Anesthesia was initiated by an intravenous injection of pentobarbital sodium (50 mg/kg) via the marginal ear vein, and then maintained at an appropriate level by continuous intravenous infusion of α-chloralose and urethane (16 mg/kg/h and 100 mg/kg/h) through a catheter inserted into the femoral vein. The animals were intubated and ventilated mechanically with room air mixed with oxygen. Systemic arterial pressure was monitored by a catheter inserted into the femoral artery. Esophageal temperature, which was measured by a thermometer (CTM-303, Terumo, Japan), was maintained between 38 and 39 °C using a heating pad. Bilateral vagal nerves were exposed through a midline cervical incision and sectioned at the neck.

With the animal in supine position, a full median sternotomy was performed to expose the heart. The right cardiac sympathetic nerve

---

[*] Corresponding author. Department of Cardiovascular Dynamics, Advanced Medical Engineering Center, National Cardiovascular Center Research Institute, 5-7-1, Fujishirodai, Suita, Osaka, 565-8565, Japan. Tel.: +81 6 6833 5012; fax: +81 6 6835 5403.
E-mail address: shujismz@ri.ncvc.go.jp (S. Shimizu).

1566-0702/$ – see front matter © 2009 Elsevier B.V. All rights reserved.
doi:10.1016/j.autneu.2009.08.017

was exposed through the sternotomy and sectioned intrathoracically. A pair of bipolar stainless steel electrodes was attached to the efferent side of the right cardiac sympathetic nerve. The nerve and electrode were immobilized using a quick-dry silicone gel (Kwik-Cast and Kwik-Sil, World Precision Instruments, Inc., FL, USA). When sympathetic stimulation was required, the efferent sympathetic nerve was stimulated by a digital stimulator (SEN-7203, Nihon Kohden, Japan), at a pulse duration of 1 ms and an amplitude of 5 V. Three stainless electrodes were attached around the incision of sternotomy for the body surface electrocardiogram. The heart rate was determined from the electrocardiogram using a cardiotachometer. Heparin sodium (100 IU/kg) was administered intravenously to prevent blood coagulation. A dialysis probe was implanted and dialysis was conducted as described in *Dialysis Technique* below. At the end of the experiment, the animal was euthanized with an overdose injection of pentobarbital sodium. In the postmortem examination, the right atrial wall was resected with dialysis fiber. We observed the inside of atrial wall macroscopically and confirmed that the dialysis membrane was not exposed to right atrial lumen.

2.2. Dialysis technique

The materials and properties of the dialysis probe have been described previously. (Akiyama et al., 1991; Shimizu et al., 2009) A dialysis fiber of semipermeable membrane (4 mm length, 310 μm outer diameter, 200 μm inner diameter; PAN-1200, 50,000 molecular weight cutoff; Asahi Chemical, Tokyo, Japan) was attached at both ends to polyethylene tubes (25 cm length, 500 μm outer diameter, 200 μm inner diameter). A fine guiding needle (30 mm length, 510 μm outer diameter, 250 μm inner diameter) with a stainless steel rod (5 mm length, 250 μm outer diameter) was used for the implantation of the dialysis probe. A dialysis probe was implanted into the right atrial myocardium near the junction between the superior vena cava and the right atrium. After implantation, the dialysis probe was perfused with Ringer's solution (NaCl 147 mM, KCl 4 mM, $CaCl_2$ 3 mM) at a speed of 2 μl/min, using a microinjection pump (CMA/102, Carnegie Medicin, Sweden). Experimental protocols were started 120 min after implantation of the dialysis probe. We took account of the dead space between the dialysis membrane and the sample tube at the start of each dialysate sampling. Four-μl phosphate buffer (pH 3.5) was transferred into each sample tube before dialysate sampling. Dialysate sampling periods were set at 10 min (1 sample volume = 20 μl). Dialysate NE concentration was analyzed by high performance liquid chromatography (Akiyama et al., 1991).

2.3. Experimental protocols

2.3.1. Protocol 1

To examine whether atrial interstitial NE level reflects NE release from cardiac sympathetic nerve endings, we investigated the effect of sympathetic nerve stimulation on dialysate NE concentration and analyzed the relationship between the dialysate NE concentrations and heart rate ($n = 7$). We sampled control dialysate after transecting the right sympathetic nerve. Then we stimulated the right sympathetic nerve for 10 min each at frequencies of 2, 5 and 10 Hz, and collected the dialysate during each stimulation. There was a 30-min interval between the different stimulation frequencies. Twenty min after sympathetic nerve stimulation, we sampled the dialysate again to check for recovery of NE level.

2.3.2. Protocol 2

Most of the released NE is removed by neuronal uptake mechanism in the heart (Goldstein et al., 1988). To examine whether an increase in atrial interstitial NE level reflects the increase in synaptic NE levels associated with inhibition of neuronal uptake, we investigated the effects of sympathetic nerve stimulation on dialysate NE concentration in the presence of neuronal uptake inhibition and analyzed the relationship between dialysate NE concentration and heart rate ($n = 7$). After intravenous administration of a neuronal uptake inhibitor, desipramine (1.0 mg/kg), we stimulated the right sympathetic nerve and sampled the dialysate in a similar fashion as in Protocol 1.

2.4. Statistical analysis

All data are presented as means ± SE. Heart rate and dialysate NE concentrations (logarithmic transformation) in response to sympathetic stimulation were compared between the absence and presence of desipramine by two-way analysis of variance (ANOVA). If there was not a significant interaction between desipramine and stimulation effects, heart rate and dialysate NE concentrations (logarithmic transformation) in response to sympathetic stimulation were compared using Dunnett's test. After logarithmic transformation of dialysate NE concentration, a linear regression analysis was performed to examine the relation between dialysate NE concentration and heart rate. The differences in slope and intercept between two regression lines were examined. (Glantz, 2005) Differences were considered significant at $P < 0.05$.

3. Results

In Protocol 1 (stimulation alone), right cardiac sympathetic nerve stimulation significantly increased heart rate from 260 ± 8 bpm in the pre-stimulation control to 298 ± 11 bpm during stimulation at 2 Hz ($P < 0.01$ vs. control), 319 ± 10 bpm at 5 Hz ($P < 0.01$ vs. control) and 318 ± 11 bpm at 10 Hz ($P < 0.01$ vs. control) (ANOVA, $P < 0.001$). Heart rate recovered to 261 ± 9 bpm 20 min after stimulation. Right cardiac sympathetic nerve stimulation significantly increased dialysate NE concentration from 0.4 ± 0.1 nM in the pre-stimulation control to 1.0 ± 0.1 nM during stimulation at 2 Hz ($P < 0.01$ vs. control), 2.2 ± 0.5 nM at 5 Hz ($P < 0.01$ vs. control) and 2.9 ± 0.9 nM at 10 Hz ($P < 0.01$ vs. control) (ANOVA, $P < 0.001$). Dialysate NE concentration recovered to the pre-stimulation level 20 min after stimulation (0.6 ± 0.1 nM) (Fig. 1).

In Protocol 2 (desipramine + stimulation), intravenous administration of desipramine significantly increased baseline heart rate (295 ± 11 vs. 263 ± 11 bpm, $P < 0.01$, paired t test) and baseline dialysate NE concentration (1.5 ± 0.2 vs. 0.8 ± 0.2 nM, $P < 0.01$, paired t test) compared

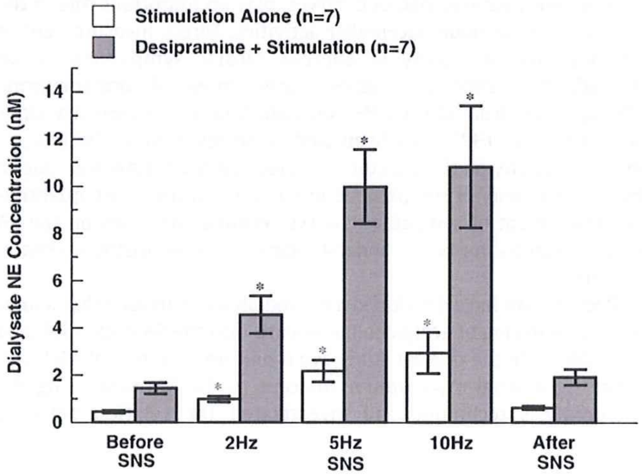

Fig. 1. Dialysate NE concentrations of controls and during electrical stimulation of right cardiac sympathetic nerve at different frequencies. The two-way analysis of variance (ANOVA) revealed the significant effect of sympathetic nerve stimulation on dialysate NE concentration ($P < 0.001$) and the significant difference in dialysate NE concentration ($P < 0.001$) between the absence and presence of desipramine. The interaction between desipramine and stimulation effects was not significant. Values are means ± SE; NE: norepinephrine; SNS: electrical sympathetic nerve stimulation; n: number of rabbits; *: $P < 0.01$ vs. the pre-stimulation control by Dunnett's test.

to Protocol 1. Right cardiac sympathetic nerve stimulation significantly increased heart rate from 295 ± 11 bpm in the pre-stimulation control to 349 ± 9 bpm during stimulation at 2 Hz ($P<0.01$ vs. control), 361 ± 8 bpm at 5 Hz ($P<0.01$ vs. control) and 351 ± 9 bpm at 10 Hz ($P<0.01$ vs. control) (ANOVA, $P<0.001$). Heart rate recovered to 295 ± 13 bpm 20 min after stimulation. Right sympathetic nerve stimulation also increased dialysate NE concentration from 1.5 ± 0.2 nM in the pre-stimulation control to 4.6 ± 0.8 nM during stimulation at 2 Hz ($P<0.01$ vs. control), 10.0 ± 1.6 nM at 5 Hz ($P<0.01$ vs. control) and 10.8 ± 2.6 nM at 10 Hz ($P<0.01$ vs. control) (ANOVA, $P<0.001$). Dialysate NE concentration recovered to the pre-stimulation level 20 min after stimulation (1.9 ± 0.3 nM) (Fig. 1). Heart rate and dialysate NE concentrations in Protocol 2 (desipramine + stimulation) were significantly higher than those in Protocol 1 (stimulation alone) (ANOVA, $P<0.001$). The interaction between desipramine and stimulation effects was not significant.

The relation between heart rate and dialysate NE concentration is shown in Fig. 2. Dialysate NE concentration correlated well with heart rate in both Protocols 1 and 2 (Protocol 1: $\mathrm{HR}=290+87\times\log[\mathrm{NE(nM)}]$, $R^2=0.71$; Protocol 2: $\mathrm{HR}=283+74\times\log[\mathrm{NE(nM)}]$, $R^2=0.70$) There was no significant difference in the intercept or slope between the two regression lines obtained from Protocols 1 and 2. (Glantz, 2005)

4. Discussion

We were able to monitor in vivo interstitial NE levels at the SA node using microdialysis technique. A neuronal uptake inhibitor, desipramine, significantly increased dialysate NE concentration in the right atrial myocardium. However, desipramine scarcely affected the relation between interstitial NE levels and heart rate.

4.1. Characteristics of dialysate NE concentration in right atrial myocardium

Dialysate NE concentration in the right atrial myocardium increased in response to electrical stimulation of the right cardiac sympathetic nerve and decreased to the pre-stimulation level after stimulation. These results indicate that atrial dialysate NE concentration reflects NE release from cardiac sympathetic nerve endings innervating the right atrium. Furthermore, a semi-log plot demonstrated a linear relationship between the right atrial dialysate NE concentration and heart rate. Judging from this relation, a 10-fold increase in dialysate NE concentration corresponds to an increase in heart rate of 87 bpm. The relative changes in NE release monitored by microdialysis correlate well with the frequency in depolarization of the SA nodal cell. Thus, we consider that dialysate NE concentration does reflect the relative changes in synaptic NE level. The relation between exogenous NE concentration and heart rate has been investigated in the isolated rabbit's atria (Toda, 1969). However, there is no report of a direct method to assess the endogenous NE release into the SA node. Microdialysis enables the monitoring of endogenous NE release into the SA node.

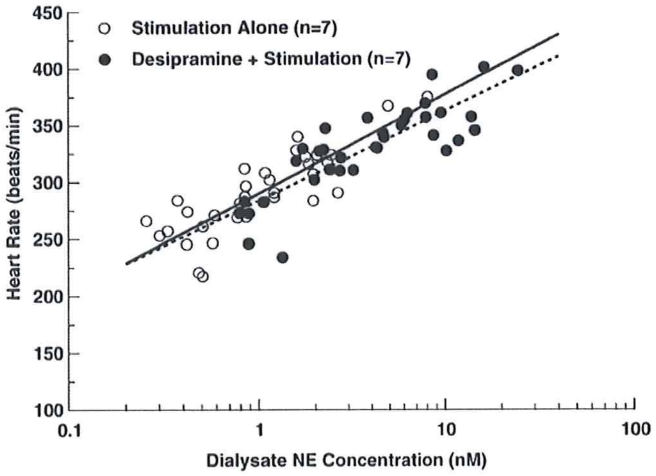

Fig. 2. Relation between dialysate NE concentration (logarithmic scale) and heart rate. Dialysate NE concentration in the right atrial myocardium correlates well with heart rate. Solid line: regression line fitting 35 data points obtained from Protocol 1 (stimulation alone) ($R^2=0.71$); dotted line: regression line fitting 35 data points obtained from Protocol 2 (desipramine + stimulation) ($R^2=0.70$). NE: norepinephrine.

4.2. Effect of neuronal uptake on dialysate NE concentration

In the presence of desipramine, a neuronal uptake inhibitor, dialysate NE concentration also increased in response to sympathetic nerve stimulation and decreased to the pre-stimulation levels after stimulation. However, dialysate NE concentrations were 3.1–4.6 times higher than the corresponding values in the absence of desipramine. These results are consistent with earlier experimental studies demonstrating that a large part of released NE is removed by neuronal uptake (Goldstein et al., 1988). In the present study, we were able to monitor the change in neuronal NE uptake function induced by desipramine using microdialysis technique.

Linked with the increase in dialysate NE concentrations in the presence of desipramine, heart rates were 33–51 bpm higher than the corresponding values in the absence of desipramine. Thus, desipramine does not alter the relation between dialysate NE concentration and heart rate. The intercept and the slope of regression line also did not differ significantly in the presence and absence of desipramine. These results indicate that neuronal uptake removes effective NE from the synaptic cleft without affecting the sensitivity of the SA nodal cell, and that neuronal NE uptake function plays an important role in the regulation of heart rate. The increase in synaptic NE concentration induced by inhibition of neuronal uptake affects the frequency of depolarization of the SA nodal cell.

Endoh (1975) reported that desipramine shifted the dose–response curve for exogenous NE to the lower NE levels. Since desipramine suppresses the neuronal uptake of both endogenous and exogenous NE, the increase in effective NE on the sinoatrial node may yield this apparent shift in the dose–response curve. Our results suggest that desipramine-inhibited neuronal uptake scarcely affects the relation between synaptic NE concentration and heart rate. Therefore, microdialysis may be a powerful tool to assess the change of synaptic NE concentration in the SA node.

4.3. Limitation

There were several limitations in the present study. First, since we did not section the left cardiac sympathetic nerve, the influence of left sympathetic nerve on the dialysate NE concentration cannot be excluded. Therefore, intravenous administration of desipramine could inhibit neuronal NE uptake at the left sympathetic nerve endings and increase dialysate NE concentration. Second, desipramine may affect the dynamic response of heart rate to sympathetic activation. We have already reported that desipramine decreases the natural frequency of the transfer function from sympathetic nerve activity to heart rate (Kawada et al., 2004). However, cardiac microdialysis using shorter dialysis fiber requires 10-min sampling time to detect changes in myocardial interstitial NE levels. Therefore, we were not able to investigate the dynamic response of heart rate to sympathetic activation in this study.

4.4. Conclusion

We were able to monitor endogenous NE release into the SA node and detect the changes in neuronal uptake function using microdialysis technique. Neuronal NE uptake together with NE release functions play an important role in the regulation of synaptic NE concentration in the SA node. Microdialysis is a powerful tool to assess the changes of synaptic NE concentration in the SA node.

Acknowledgements

This study was supported by Health and Labor Sciences Research Grants (H18-nano-Ippan-003, H19-nano-Ippan-009, H20-katsudo-Shitei-007 and H21-nano-Ippan-005) from the Ministry of Health, Labor and Welfare of Japan, by Grants-in-Aid for Scientific Research (No. 20390462) from the Ministry of Education, Culture, Sports, Science and Technology in Japan and by the Industrial Technology Research Grant Program from New Energy and Industrial Technology Development Organization (NEDO) of Japan.

References

Akiyama, T., Yamazaki, T., Ninomiya, I., 1991. In vivo monitoring of myocardial interstitial norepinephrine by dialysis technique. Am. J. Physiol. 261, H1643–H1647.

Endoh, M., 1975. Effects of dopamine on sinus rate and ventricular contractile force of the dog heart in vitro and in vivo. Br. J. Pharmacol. 55, 475–486.

Glantz, S.A., 2005. Primer of Biostatistics, 6th ed. McGraw-Hill, New York.

Goldstein, D.S., Brush Jr., J.E., Eisenhofer, G., Stull, R., Esler, M., 1988. In vivo measurement of neuronal uptake of norepinephrine in the human heart. Circulation 78, 41–48.

Kawada, T., Miyamoto, T., Uemura, K., Kashihara, K., Kamiya, A., Sugimachi, M., Sunagawa, K., 2004. Effects of neuronal norepinephrine uptake blockade on baroreflex neural and peripheral arc transfer characteristics. Am. J. Physiol. Regul. Integr. Comp. Physiol. 286, R1110–R1120.

Meredith, I.T., Eisenhofer, G., Lambert, G.W., Dewar, E.M., Jennings, G.L., Esler, M.D., 1993. Cardiac sympathetic nervous activity in congestive heart failure. Evidence for increased neuronal norepinephrine release and preserved neuronal uptake. Circulation 88, 136–145.

Shimizu, S., Akiyama, T., Kawada, T., Shishido, T., Yamazaki, T., Kamiya, A., Mizuno, M., Sano, S., Sugimachi, M., 2009. In vivo direct monitoring of vagal acetylcholine release to the sinoatrial node. Auton. Neurosci. 148, 44–49.

Toda, N., 1969. Interactions of ouabain and noradrenaline in isolated rabbit's atria. Br. J. Pharmacol. 36, 393–408.

31st Annual International Conference of the IEEE EMBS
Minneapolis, Minnesota, USA, September 2-6, 2009

Preliminary Study on the Detection of Cardiac Arrhythmias based on Multiple Simultaneous Electrograms

Telma Keiko Sugai, Student Member, *IEEE*, Makoto Yoshizawa, Member, *IEEE*,
Makoto Abe, Student Member, *IEEE*, Kazuo Shimizu, Masashi Inagaki, Member *IEEE*,
Masaru Sugimachi, Member *IEEE*, and Kenji Sunagawa, Member *IEEE*

Abstract— **Although implantable cardioverter-defibrillators have improved significantly in the past decades, the algorithms used in the identification of life-threatening arrhythmias are still not accurate enough. Conventional methods commonly misclassify tachycardias, sometimes initiating an unnecessary and uncomfortable treatment. In this paper, we proposed a new method for the identification of ventricular tachycardias and fibrillations based on the comparison of simultaneous electrograms. Our method could successfully separate supraventricular tachycardias and normal sinus rhythm, which do not require any treatment, from ventricular tachycardias and fibrillation, which are life-threatening arrhythmias and must be terminated, with a sensitivity of 93.0% and a specificity of 92.7% from the comparison of ventricular electrograms. In future studies, the classification using electrograms from the right heart must be improved.**

I. INTRODUCTION

Each year in the United States, about 450,000 people die of unexpected sudden cardiac death [1]. Further, it is known that the risk of a recurrence is high in survivors of sudden cardiac death. Therefore, in patients at risk for recurrent sustained ventricular tachycardia (VT) or fibrillation (VF), implantable cardioverter defibrillators (ICDs) are used to automatically deliver electrical shocks in order to restore the normal rhythm.

The ICDs have been used for more than 2 decades; in this period they have improved substantially becoming highly effective in terminating malignant arrhythmias. However the detection of life-threatening arrhythmias still lacks accuracy. Delivery of inappropriate shocks, commonly related to the misclassification of a supraventricular tachycardia (SVT) as a VT, can lead to pain, anxiety, depression, impaired quality of life, proarrhythmia, and poor tolerance of life-saving ICD therapy [2], [3], [4], [5], [6].

On the other hand, the long ICD lifetime operating with typical batteries demands very low power consumption by the ICD microprocessor, which limits the use of complex detection algorithms [3].

Conventionally, ventricular arrhythmias are detected either based on the heart rate or based on the electrograms (EGMs) morphology. One example of criterion based on the heart rate is to use programmable thresholds to discriminate the arrhythmias since during a VF the heart rate is higher than during a VT, and during a VT the heart rate is higher than during a normal sinus rhythm (SR). The morphologic criterion is based on comparing the EGM morphology with a sample of pre-stored EGMs of each arrhythmia. However, both heart rate and EGM morphology are not stable, which makes it difficult to define a threshold or a particular morphology for each arrhythmia.

In this paper we propose a method for detection of ventricular arrhythmias based on the comparison of simultaneous EGMs from the left ventricle (EGM_{LV}), the right ventricle (EGM_{RV}) and the right atrium (EGM_{RA}). Preliminary results indicate that this algorithm permits earlier classification of the cardiac rhythm and with a lower computational cost than the conventional methods; however, further comparative studies are necessary. During the SR or during a SVT, the excitation is transmitted from the atrium to both ventricles through the His-Purkinje bundle; therefore, the EGM of both ventricles are synchronized with each other and with the EGM_{RA}. On the other hand, VTs and VFs are caused by an ectopic electrical excitation in the ventricle which is not transmitted through the His-Purkinje bundle causing the ventricular electrograms to be independent of each other and also of the EGM_{RA}.

II. METHODS

A. Data Description

In this study *in vivo* data were obtained from a dog in an acute experiment. EGMs were measured from leads in the left and right ventricles and right atrium and sampled at 250Hz. SVT was simulated by right atrial pacing. VT was simulated by right or left ventricular pacing. And VF was induced by electrical stimuli after the R-wave of the surface electrocardiogram. The distribution of the episodes and the length of the data of each rhythm are detailed in Table I.

This work was supported by the Grant of Tohoku University Global COE Program: Global Nano-Biomedical Engineering Education and Research Network Center and by the Grant-In-Aid of Scientific Research of Japanese Ministry of Health, Labor and Welfare.

T.K. Sugai is with Graduate School of Biomedical Engineering, Tohoku University, 6-6-05, Aoba, Aramaki, Aoba-ku, Sendai 980-8579, Japan. `telma@yoshizawa.ecei.tohoku.ac.jp`

M. Yoshizawa and M. Abe are with Cyberscience Center, Tohoku University, Sendai, Japan.

K. Shimizu is with Olympus Corp., Tokyo, Japan.

M. Inagaki and M. Sugimachi are with Department of Cardiovascular Dynamics, Research Institute of National Cardiovascular Center, Osaka, Japan.

Kenji Sunagawa is with Graduate School of Medicine, Kyushu University, Fukuoka, Japan

978-1-4244-3296-7/09/$25.00 ©2009 IEEE

TABLE I

NUMBER OF EPISODES AND TOTAL DURATION OF THE DATA OF EACH RHYTHM

	Number of Episodes	Total Duration [s]
SR	14	179.2
SVT	5	41.6
VT	7	61.4
VF	4	40.6

B. Preprocessing

The data were analyzed in a moving data window with 1.0s length and 0.2s shift. Before the analysis, the signals were band-pass filtered between 0.8Hz and 35Hz to reduce noise and remove the baseline. Next, the relative distribution of each pair of EGMs was extracted from two dimensional histograms with 5x5 bins. In Fig. 1 are represented examples of histograms of EGM_{LV} versus EGM_{RV} for the SR and for some arrhythmias.

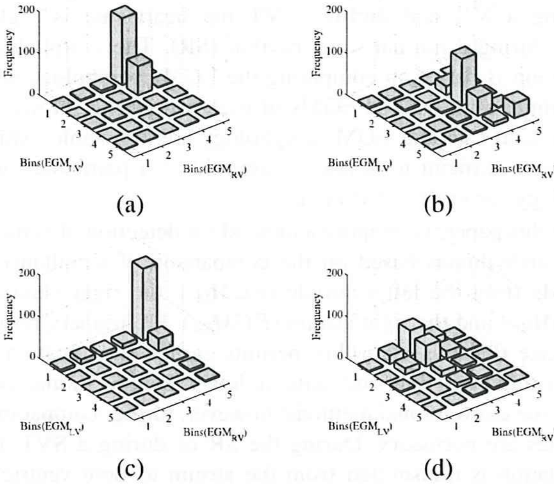

Fig. 1. Histograms representing relative distribution of EGM_{LV} and EGM_{RV} during (a) SR, (b) SVT, (c) VT and (d) VF

C. Classification

The classification was based on a decision tree using the Pearson's χ^2 statistic and the variation of the histograms. The first index was used to separate SRs and SVTs from VTs and VFs, while the second one was used to separate VTs from VFs.

The Pearson's χ^2 statistic was used to test the null hypothesis that the EGM_{LV} and the EGM_{RV}, or the EGM_{RA} and the EGM_{RV}, are independent, which is false in SRs and SVTs. The value of the test statistic χ^2 is

$$\chi^2 = \sum_{i=1}^{n_i} \sum_{j=1}^{n_j} \frac{(O_{ij} - E_{ij})^2}{E_{ij}}, \qquad (1)$$

where O_{ij} is an observed frequency, E_{ij} is the expected frequency if confirmed the null hypothesis and n is the number of possible outcomes of each event.

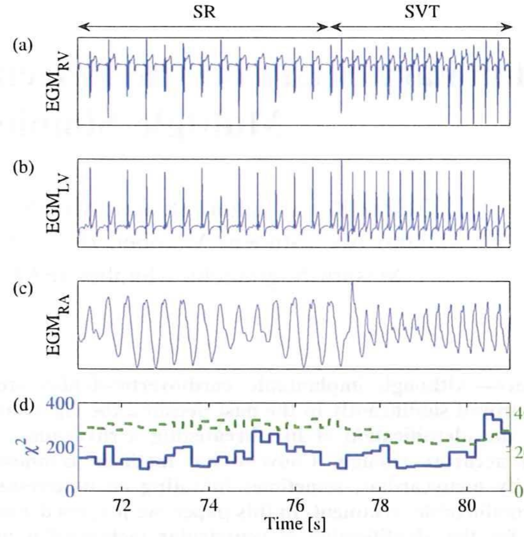

Fig. 2. Example of (a) EGM_{RV}, (b) EGM_{LV}, (c) $EGM_{RA}$and (d) the calculated χ^2 statistic (continuous line) and dispersion σ (dashed line) during a SVT episode.

We calculated the χ^2 using (2) approximating the joint probability distribution ($p(a_i,b_j)$) to the frequency of each bin of the histogram and the probability distribution corresponding to each EGM ($p(a_i)$ and $p(b_j)$) to the sum of the frequency of each column and each row, respectively.

$$\chi^2 = \sum_{i=1}^{5} \sum_{j=1}^{5} \frac{(p(a_i,b_j) - p(a_i) \cdot p(b_j))^2}{p(a_i) \cdot p(b_j)}. \qquad (2)$$

Next, the dispersion of the histogram of two EGMs was used to identify VFs. The dispersion of the histogram was calculated as the standard deviation (σ) of the counts in each bin of the histogram, as in (3).

$$\sigma = \frac{1}{n_a \cdot n_b} \sum_{i=1}^{n_a} \sum_{j=1}^{n_b} (p(a_i,b_j) - \mu)^2, \qquad (3)$$

where μ is the mean of $p(a_i,b_j)$.

The classification was validated using a 10-fold cross validation. The training and validation sets were separated maintaining a constant rate of 9:1 samples of each rhythm. The thresholds were interactively defined as the value that maximizes the sensitivity and the specificity of the classification of the training set.

III. RESULTS

Figs. 2, 3 and 4 show examples of EGMs and the calculated indices during the transition to a SVT, a VT and a VF episode, respectively. In the top three graphs ((a), (b) and (c)) of each figure are represented segments of EGMs acquired simultaneously from the right ventricle, left ventricle and right atrium. In the bottom graph (d) of each figure are shown the values of the indices used for the classification: χ^2-statistic and σ, extracted from the ventricular EGMs represented in the top graphs.

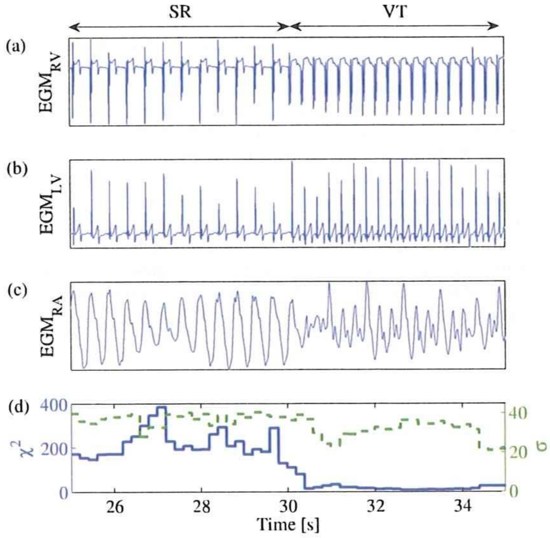

Fig. 3. Example of (a) EGM_{RV}, (b) EGM_{LV}, (c) EGM_{RA} and (d) the calculated χ^2 statistic (continuous line) and dispersion σ (dashed line) during a VT episode.

TABLE II

PERFORMANCE OF THE CLASSIFIER USING EGM_{LV} AND EGM_{RV} (VENTRICULAR ARRHYTHMIAS VS. OTHER RHYTHMS)

	VT or VF	SR or SVT
Shock	TP = 549	FP = 86
Ignore	FN = 41	TN = 1104
	Sensitivity = 93.0%	Specificity = 92.7%

The results from the validation of the classifier are shown in Tables II - V. In the classification using both ventricular EGMs, EGM_{LV} and EGM_{RV}, the mean (± standard deviation) threshold for the χ^2 was 76.4 (± 1.9) and the mean threshold for the σ was 16.8 (± 0.3). In the classification using ECGs from the right heart, EGM_{RA} and EGM_{RV}, the mean (± standard deviation) threshold for the χ^2 was 61.1 (± 0.9) and the mean threshold for the σ was 13.2 (± 0.2).

The sensitivity and specificity of the classifier were calculated from the sum of the respective true positive (TP), false positive (FP), false negative (FN) and true negative (TN) of each interaction of the cross validation. The detailed results of the detection of life-threatening arrhythmias, by separating VTs and VFs from SVTs and SRs, are shown in Tables II and IV. The results of the decision of whether the ICD should apply a shock to recover from a VF, or start pacing to recover from a VT, are detailed in Tables III and V.

The results presented in Tables II and III correspond to the classification based on the EGM_{LV} and the EGM_{RV}, which are available only in biventricular ICDs. The results presented in Tables IV and V correspond to the classification based on the EGM_{RA} and the EGM_{RV}, which are available also in dual chamber ICDs.

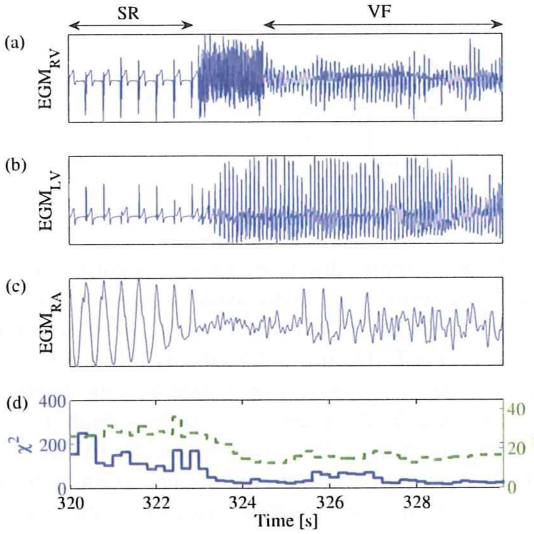

Fig. 4. Example of (a) EGM_{RV}, (b) EGM_{LV}, (c) EGM_{RA} and (d) the calculated χ^2 statistic (continuous line) and dispersion σ (dashed line) during a VF episode.

TABLE III

PERFORMANCE OF THE CLASSIFIER USING EGM_{LV} AND EGM_{RV} (VT VS. VF)

	VF	VT
Shock	TP = 229	FP = 7
Pacing	FN = 10	TN = 303
	Sensitivity = 95.8%	Specificity = 97.7%

IV. DISCUSSION

Conventional methods for the discrimination of the cardiac rhythms have a special limitation for the separation between SVTs and VTs. Studies using morphology-based algorithms have reported higher specificity and sensitivity in this detection, however it was still necessary to have a more accurate method that could fit the low computational cost requirements of an ICD [5].

In this paper, we proposed a new algorithm for the detection of arrhythmias for ICDs. On the basis of the comparison of EGMs, VF and VT were separated from SVT or SR by the comparison of the independence of the two simultaneous EGMs. It was observed that during the normal SR, and also during SVT, there was a high similarity especially between the EGM_{LV} and the EGM_{RV}, which decreased during ventricular arrhythmias. Dependencies are commonly measured using mutual information or χ^2 statistics; in this study, we

TABLE IV

PERFORMANCE OF THE CLASSIFIER USING EGM_{RA} AND EGM_{RV} (VENTRICULAR ARRHYTHMIAS VS. OTHER RHYTHMS)

	VT or VF	SR or SVT
Shock	TP = 439	FP = 318
Ignore	FN = 151	TN = 872
	Sensitivity = 74.4%	Specificity = 73.3%

TABLE V
PERFORMANCE OF THE CLASSIFIER USING EGM_{RA} AND EGM_{RV} (VT VS. VF)

	VF	VT
Shock	TP = 223	FP = 1
Pacing	FN = 26	TN = 189
	Sensitivity = 89.6%	Specificity = 99.5%

choose the χ^2 statistics due to its lower computational cost.

Once a life-threatening arrhythmia is detected, the ICD must apply a shock, if rhythm is a VF, or start pacing, if rhythm is a VT. During a VF, the EGMs have higher frequencies and are desynchronized; therefore, the dispersion of one ventricular EGM against the another is high. Using a two-dimensional histogram of two ventricular EGMs, or of two EGMs from the right heart, the dispersion was extracted from the deviation of the frequency in each of the bins.

A 10-fold cross-validation showed that the method has a high sensibility and specificity even in the separation of SVTs from VTs when using ventricular EGMs. However, EGMs of both ventricles are not usually acquired in dual-chamber ICDs. The results of the classification using EGMs from the right heart showed a poor separation of SVTs and VTs. These results are expected to be improved when accounting information from past windows. For instance, during a SVT if some isolated samples was classified as VT, the classification as a VT is probably wrong. The low standard deviation of the threshold during the cross validation reflects the stability of the chosen indices.

These results were obtained from a limited data set. The algorithm must be evaluated in more data from different conditions. The use of indices obtained from histograms has the advantage to be independent of the signal amplitude. Therefore, it is expected to be more robust, for example, to differences among patients and to patients activities.

V. CONCLUSIONS AND FUTURE WORKS

In a limited dataset, this preliminary study showed the possibility to detect life-threatening arrhythmias from the comparison of simultaneous electrograms by the extraction of the independence of electrograms using the χ^2 statistic and of the relative dispersion of electrograms using the standard deviation of their joint probability.

In future studies, other features should be extracted from the EGM_{RV} and EGM_{RA}, such as phase synchronization and delay or relative period, in order to improve the classification using EGMs from the right heart only, which would permit the application of this algorithm not only in biventricular ICDs but also in dual-chamber ICDs.

REFERENCES

[1] "State-specific mortality from sudden cardiac death - united states, 1999," *MMWR Weekly February 15*, vol. 51, no. 06, pp. 123–126, 2002.

[2] C. W. Israel, "How to avoid inappropriate therapy," *Current Opinion in Cardiology*, vol. 23, p. 65.71, 2008.

[3] A. Cebrian, J. Millet, and F. Castells, "Implantable cardioverter defibrillator algorithms: status review in terms of computational cost," *Biomed Tech (Berl)*, vol. 52, no. 1, pp. 25–30, 2007.

[4] P. A. Friedman, R. L. McClelland, W. R. Bamlet, H. Acosta, D. Kessler, T. M. Munger, N. G. Kavesh, M. Wood, E. Daoud, A. Massumi, C. Schuger, S. Shorofsky, B. Wilkoff, and M. Glikson, "Dual-chamber versus single-chamber detection enhancements for implantable defibrillator rhythm diagnosis the detect supraventricular tachycardia study," *Circulation*, vol. 113, no. 25, pp. 2871–2879, 2006.

[5] E. Aliota, R. Nitzsche, and A. Ripart, "Arrhythmia detection by dual-chamber implantable cardioverter defibrillators: A review of current algorithms," *Europace*, vol. 6, pp. 273–286, 2004.

[6] D. A. Theuns, M. Rivero-Ayerza, E. Boersma, and L. Jordaens, "Prevention of inappropriate therapy in implantable defibrillators: A meta-analysis of clinical trials comparing single-chamber and dual-chamber arrhythmia discrimination algorithms," *International Journal of Cardiology*, vol. 125, no. 3, pp. 352 – 357, 2008.

Circ J 2009; **73:** 1395–1396

Coronary Artery Volume Noninvasively Measured With Multislice Computed Tomography

—— Definition, Accuracy and Implication ——

Masaru Sugimachi, MD; Toru Kawada, MD

In this issue of *Circulation Journal*, Ehara et al[1] describe a new concept of measuring 'coronary artery volume' (CAV) to examine the balance between coronary vasculature and myocardial mass. They have developed a method of measuring CAV as accurately as possible using 64-slice computed tomography (64-MSCT). An adaptive threshold value was used to detect the coronary artery border to improve the accuracy of CAV. Ehara et al have exemplified the usefulness of CAV by examining the relationship between CAV and left ventricular mass (LVM) in consecutive patients undergoing MSCT without significant coronary artery stenosis or left ventricular wall motion abnormality. The authors concluded that CAV increases with LVM, but that the increase was not sufficient for the increase in LVM.

Article p 1448

What is CAV?

The authors have defined CAV as the sum of the small volumes opacified by the contrast medium. The opacified small volumes were detected by the difference of radiodensity or Hounsfield unit (an index showing the degree of transparency to X-ray) using 64-MSCT (see below for details). Because the authors have analyzed data of routine 64-MSCT for the evaluation of coronary artery disease, the image is taken when the arterial side is mainly opacified, during the diastolic cardiac phase, and under coronary vasodilatation. Therefore, CAV mainly represents the sum of volumes of epicardial coronary arteries larger than the arteries undetectable due to the limited resolution of MSCT (see below).

How Accurate and Reproducible is CAV Measurement?

In this article, the authors have established a method of measuring CAV with every attempt to improve the accuracy and reproducibility for their MSCT device. These procedures are worthy of being discussed for other researchers who are interested in and would like to reproduce CAV measurement.

Inaccuracies and variability of CAV measurement would arise from (1) an arbitrary cut-off value for border detection, (2) partial volume effect, (3) motion artifact and (4) possible variable resolution of various MSCT devices. The authors have wisely minimized the errors introduced by the first 3 factors.

It is usually difficult to determine the border of the coronary arteries with a reasonable criterion. This may be because opacification of arteries is incomplete, or the opacification is thinner near the border than the center, resulting in a gradual decrease in radiodensity at the border, rather than a clear-cut abrupt change in radiodensity. In addition, at the border of small arteries, a voxel (the smallest size identified by 64-MSCT) may contain both arterial lumen (which is opacified) and arterial wall (which is not opacified). A voxel has a radiodensity of an intermediate value between an opacified and unopacified voxel, which is known as the 'partial volume effect'.

To minimize the errors introduced by an arbitrary cut-off value and the partial volume effect, the authors have developed a way of reasonably determining the cut-off value for border detection, based on preliminary phantom experiments with moving cylinders containing various concentrations of contrast medium. The results of these preliminary experiments are summarized in Figures 1–3 in Ehara et al[1] Figure 2 clearly shows that a cut-off value that exactly reproduces the phantom cylinder volume can be determined. The cut-off value is, however, not fixed, but changes with the true radiodensity of the contrast medium in the cylinder. Based on this, the authors determined the cut-off value for CAV measurement, adaptively in each subject, in reference to the radiodensity of the proximal region of the left and right coronary arteries. The cut-off value was not relatively influenced by different heart rates, which also decreased the degree of error by motion artifacts. Similar procedures may be applicable to quantitative coronary angiography.

The determined threshold is, however, only valid for the specific MSCT device used in the study by Ehara et al[1] If other researchers are to reproduce their CAV measurement, another attempt to determine the threshold for their device is necessary.

The limited resolution of MSCT would determine the definition of CAV. The authors used MSCT with an isotropic resolution of 400μm. This indicates that CAV in the paper by Ehara et al would be the sum of volume of the arteries >400μm. If MSCT is used with a different resolution, the definition of CAV would be different and CAV would be systematically different.

(Received June 17, 2009; accepted June 17, 2009)

Department of Cardiovascular Dynamics, Advanced Medical Engineering Center, National Cardiovascular Center Research Institute, Suita, Japan
Mailing address: Masaru Sugimachi, MD, Department of Cardiovascular Dynamics, Advanced Medical Engineering Center, National Cardiovascular Center Research Institute, 5-7-1 Fujishirodai, Suita 565-8565, Japan. E-mail: su91mach@ri.ncvc.go.jp

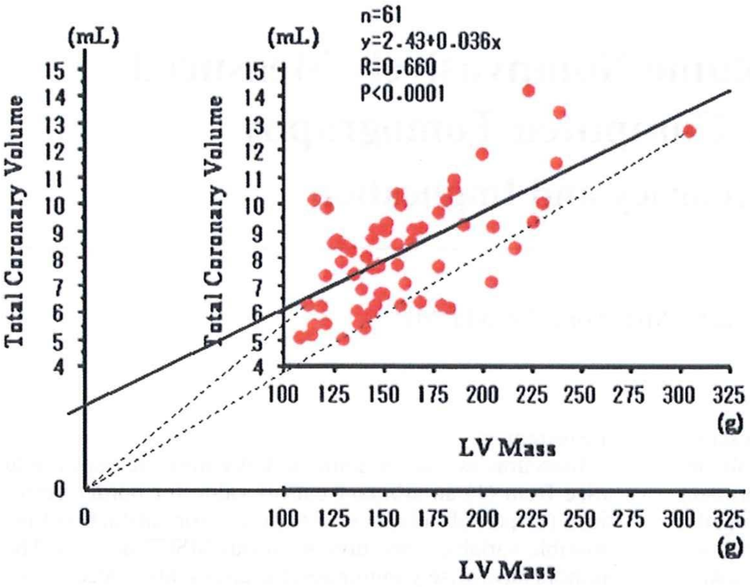

Figure. Linear regression between coronary artery volume (total coronary volume) and left ventricular (LV) mass (reproduced and modified from Ehara et al[1]). The axes are extended and the regression line is extrapolated to show a positive offset of coronary artery volume. Schematically, the authors have compared the slopes of dashed lines.

Is CAV a Proxy for Capillary Density or Coronary Flow Reserve?

The relation between coronary vasculature and myocardial mass, or more specifically inappropriate perfusion of the myocardium, has been traditionally examined histologically[2] by capillary density. Later, similar information was obtained in vivo by the measurement of coronary flow reserve. In fact, some have described the relationship between coronary capillary density and coronary flow reserve in patients with hypertrophic cardiomyopathy,[3] in patients with idiopathic dilated cardiomyopathy,[4] or in mini pigs with hypercholesterolemia.[5]

In contrast, the way in which CAV correlates with coronary capillary density or coronary flow reserve is yet to be determined. As CAV measures the volume of arteries far larger than capillaries, these problems need to be resolved (eg, by animal experiments) before we can measure CAV in patients with a wide variety of cardiovascular diseases.

It is also reasonable to assume CAV may provide information other than coronary capillary density or coronary flow reserve. In Ehara et al, CAV is only measured under nitroglycerine. The response of CAV to increased coronary flow or to endothelium-dependent vasodilatation may be of clinical value. If better accuracy and reproducibility is established, CAV may potentially replace quantitative coronary angiography for this purpose because of its noninvasive nature.

Is CAV Really Unmatched With LVM?

The authors' conclusion of unmatched CAV with LVM should be discussed. **Figure** shows the linear regression between CAV and LVM reproduced and modified from Figure 6 of Ehara et al. The modified figure has extended axes and the extrapolated regression line has been added.

Even though there is only a single data set for each patient, the authors assumed that the line started at the origin and calculated the slope. Schematically, they have compared the slopes of dashed lines.

Figure, however, indicates that the CAV–LVM relationship obtained from pooled data has a positive CAV offset, but does note indicate that the slope is shallow. Because there is no reason to deny the presence of a positive CAV offset, and because the slope was not compared with a standard slope, the conclusion of unmatched CAV with LVM is not solid.

This question may be resolved by comparing the CAV–LVM relationship obtained by sequential CAV measurement during physiological growth and that obtained during the progression of pathological hypertrophy of the heart in animal experiments.

Advantage of CAV Measurement

The noninvasive nature of CAV measurement enhances its clinical usefulness because it enables sequential evaluation and may help to bring evaluations still in the investigational stage into routine bedside practice. Similar technological developments (eg, coronary flow reserve by cine magnetic resonance[6]) may be combined and eventually enable the detailed pathophysiology of cardiovascular disease to be described.

References

1. Ehara S, Okuyama T, Shirai N, Sugioka K, Oe H, Itoh T, et al. Inadequate increase in the volume of major epicardial coronary arteries compared with that in left ventricular mass: Novel concept for characterization of coronary arteries using 64-slice computed tomography. *Circ J* 2009; **73:** 1448–1453.
2. Tomanek RJ, Wessel TJ, Harrison DG. Capillary growth and geometry during long-term hypertension and myocardial hypertrophy in dogs. *Am J Physiol* 1991; **261:** H1011–H1018.
3. Krams R, Kofflard MJ, Duncker DJ, Von Birgelen C, Carlier S, Kliffen M, et al. Decreased coronary flow reserve in hypertrophic cardiomyopathy is related to remodeling of the coronary microcirculation. *Circulation* 1998; **97:** 230–233.
4. Tsagalou EP, Anastasiou-Nana M, Agapitos E, Gika A, Drakos SG, Terrovitis JV, et al. Depressed coronary flow reserve is associated with decreased myocardial capillary density in patients with heart failure due to idiopathic dilated cardiomyopathy. *J Am Coll Cardiol* 2008; **52:** 1391–1398.
5. Theilmeier G, Verhamme P, Dymarkowski S, Beck H, Bernar H, Lox M, et al. Hypercholesterolemia in minipigs impairs left ventricular response to stress: Association with decreased coronary flow reserve and reduced capillary density. *Circulation* 2002; **106:** 1140–1146.
6. Sakuma H, Koskenvuo JW, Niemi P, Kawada N, Toikka JO, Knuuti J, et al. Assessment of coronary flow reserve using fast velocity-encoded cine MR imaging: Validation study using positron emission tomography. *Am J Roentgenol* 2000; **175:** 1029–1033.

31st Annual International Conference of the IEEE EMBS
Minneapolis, Minnesota, USA, September 2-6, 2009

Feedback Control of Multiple Hemodynamic Variables with Multiple Cardiovascular Drugs

Masaru Sugimachi, *Member, IEEE*, Kazunori Uemura,
Atsunori Kamiya, Shuji Shimizu, Masashi Inagaki, and Toshiaki Shishido

Abstract— **The ultimate goal of disease treatment is to control the biological system beyond the native regulation to combat pathological process. To maximize the advantage of drugs, we attempted to pharmacologically control the biological system at will, e.g., control multiple hemodynamic variables with multiple cardiovascular drugs. A comprehensive physiological cardiovascular model enabled us to evaluate cardiovascular properties (pump function, vascular resistance, and blood volume) and the feedback control of these properties. In 12 dogs, with dobutamine (5±3 $\mu g \cdot kg^{-1} \cdot min^{-1}$), nitroprusside (4±2 $\mu g \cdot kg^{-1} \cdot min^{-1}$), dextran (2±2 $ml \cdot kg^{-1}$), and furosemide (10 mg in one, 20 mg in one), rapid, sufficient and stable control of pump function, vascular resistance and blood volume resulted in similarly quick and stable control of blood pressure, cardiac output and left atrial pressure in 5±7, 7±5, and 12±10 minutes, respectively. These variables remained stable for 60 minutes (RMS 4±3 mmHg, 5±2 $ml \cdot min^{-1} \cdot kg^{-1}$, 0.8±0.6 mmHg, respectively).**

I. INTRODUCTION

THE ultimate goal of disease treatment is to control the biological system beyond the native regulation to combat pathological process. This control may be partly achieved by native regulatory systems, but these frequently fail when disease progresses.

Many pharmacological treatments have provided us with control measures that may act in ways not possible by native regulators. To fully take advantage of these medicines, we must establish ways of using these agents to control the biological system at our will. As an example, we tried to control multiple hemodynamic variables with multiple cardiovascular drugs.

Several closed-loop systems have succeeded in directly controlling a single hemodynamic variable [1,2]. Multiple-variable control, however, has been unsuccessful [3-5].

Multiple-input multiple-output feedback control remains a challenge if the input-output relationships for all combinations are of equal significance. We therefore tried to decouple the input-output relationships by using a comprehensive physiological cardiovascular model. The model enabled us to define a set of parallel independent relationships between cardiovascular properties and drugs: pump function / inotrope, vascular resistance / vasodilator, and blood volume / volume expander. The model also provided us with a method to quantitatively calculate cardiovascular properties.

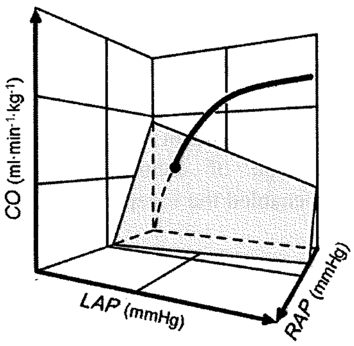

Fig. 1. Extended Guyton's model.
Thick curve, pump function of left and right heart; shaded surface, capacitive function of total vascular beds; CO, cardiac output; LAP, left atrial pressure; RAP, right atrial pressure.

II. MODEL AND METHODS

A. Cardiovascular property identification

Abnormalities of hemodynamic variables arise from abnormalities of cardiovascular properties, including pump function, vascular resistance, and blood volume. We identified these properties using an extended version of Guyton's circulatory equilibrium framework (Fig. 1) [6,7].

Pump function of the left heart (S_L) can be quantified as the ratio of cardiac output (CO) to the logarithm of left atrial pressure (LAP) ($S_L = CO / [\ln(LAP - 2.03) + 0.80]$). Systemic vascular resistance (R) can be calculated as blood pressure (BP) minus right atrial pressure (RAP) divided by CO. Stressed total blood volume (V) is obtained by $V = (CO + 19.61\ RAP + 3.49\ LAP) \times 0.129$.

B. Autopilot System

Autopilot controller of multiple hemodynamic variables consisted of multiple feedback loops. We designed these

Manuscript received April 7, 2009. This work was supported in part by Grant-in-Aid for Scientific Research (B 20300164, C 20500404) from the Ministry of Education, Culture, Sports, Science and Technology, by Health and Labour Sciences Research Grants (H19-nano-ippan-009, H20-katsudo -shitei-007) from the Ministry of Health, Labour and Welfare of Japan.

M. Sugimachi, K. Uemura, A. Kamiya, S. Shimizu, M. Inagaki, and T. Shishido are with the National Cardiovascular Center Research Institute, Suita, Osaka 5658565, Japan (corresponding author Masaru Sugimachi to provide phone: +81-6-6833-512; fax: +81-6-6835-5403; e-mail: su91mach@ri.ncvc.go.jp).

978-1-4244-3296-7/09/$25.00 ©2009 IEEE

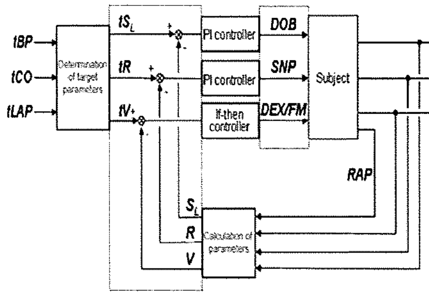

Fig. 2. Autopilot controller.
Calculated cardiovascular properties, rather than hemodynamic variables, were feedback-controlled to achieve multiple independent control of variables.

feedbacks as being independent of each other. The selection and the combination of controlled property and the controlling drugs enabled the independent operation (Fig. 2) [8].

S_L and R were controlled by proportional-integral (PI) feedback, with infusion of dobutamine (DOB) and sodium nitroprusside (SNP), respectively. Proportional and integral gain values were calculated using Chien-Hrones-Reswick's method [9] from gain, time constant, and dead-time delay of the approximated first-order step responses of S_L to DOB and R to SNP. We infused 10% dextran 40 solution (DEX, 10 $ml \cdot min^{-1}$) as long as V was <1 $ml \cdot kg^{-1}$ than the target, and injected furosemide (FM, 10 mg) every 20 minutes while V was >2 $ml \cdot kg^{-1}$ than the target.

C. Animal Experiments

We evaluated the performance of the autopilot controller in 12 adult anesthetized mongrel dogs (both sexes, 25±4 kg). We measured BP, CO, LAP and RAP. DOB, SNP, and DEX were automatically administered into the femoral vein through independent infusion routes, using either a computer-controlled roller pump or an infusion pump. FM was given through the jugular vein manually according to computer instructions.

These dogs underwent coronary microembolization, resulting in left ventricular failure. After hemodynamic stabilization, we began implementing control using the autopilot system.

III. RESULTS

	Proportional gain (K_p) $\mu g \cdot ml^{-1}$	Integral gain (K_I) sec^{-1}
S_L control	0.06	0.01
R control	-1.37	0.007

Table 1. Selected gain parameters for designed controller.
Dose ($\mu g \cdot kg^{-1} \cdot min^{-1}$) of drugs for the control of S_L (DOB) or R (SNP) is determined as (Dose) = $K_p (1 + K_I / s)\, \Delta$(Controlled variable)

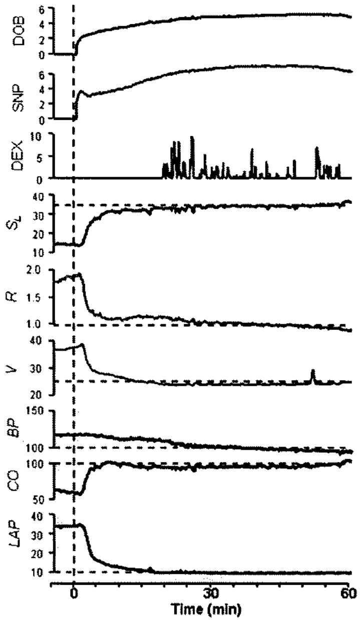

Fig. 3. An example of the automatic control of hemodynamics.
Feedback control was rapid, sufficient, and stable. DOB, dobutamine ($\mu g \cdot kg^{-1} \cdot min^{-1}$); SNP, sodium nitroprusside ($\mu g \cdot kg^{-1} \cdot min^{-1}$); DEX, dextran 40 solution ($ml \cdot min^{-1}$); S_L, pump function ($ml \cdot kg^{-1} \cdot min^{-1}$); R, resistance ($mmHg \cdot ml^{-1} \cdot kg \cdot min$); V, blood volume ($ml \cdot kg^{-1}$); BP, blood pressure (mmHg); CO, cardiac output ($ml \cdot kg^{-1} \cdot min^{-1}$); LAP, left atrial pressure (mmHg)

Based on the step response from coronary microembolized dogs, we determined the proportional and integral gain as shown in Table 1.

Similar to the example shown in Figure 3, in 12 dogs, by administering DOB (5±3 $\mu g \cdot kg^{-1} \cdot min^{-1}$), SNP (4±2 $\mu g \cdot kg^{-1} \cdot min^{-1}$), DEX (2±2 $ml \cdot kg^{-1}$), and FM (10 mg in one, 20 mg in one), rapid, sufficient and stable control of S_L, R and V. This resulted in corresponding appropriate control of BP, CO and LAP in 5±7, 7±5, and 12±10 minutes, respectively. These remained stable for 60 minutes (RMS BP=4±3 mmHg, CO=5±2 $ml \cdot min^{-1} \cdot kg^{-1}$, LAP=0.8±0.6 mmHg).

IV. DISCUSSION

We have shown that by evaluating cardiovascular properties (pump function, vascular resistance, and blood volume), and then controlling these properties with individually selected drugs, we were able to automatically control multiple hemodynamic abnormalities rapidly, stably, and simultaneously.

Direct control of multiple hemodynamic variables, however, likely fails because each drug affects more than one variable. Direct control remains unfeasible even with more complicated methods developed in control engineering; appropriate physiological modeling and precise evaluation of cardiovascular properties are essential to achieving adequate control.

V. CONCLUSION

Calculating cardiovascular properties (pump function, vascular resistance, and blood volume) based on a comprehensive cardiovascular model and feedback control of these properties are required for the accurate control of multiple hemodynamic variables (BP, CO, LAP).

REFERENCES

[1] W. R. Chitwood, Jr, D. M. Cosgrove III, R. M. Lust, "Multicenter trial of automated nitroprusside infusion for postoperative hypertension. Titrator Multicenter Study Group," *Ann. Thorac. Surg.* Vol. 54, 517–522, 1992.

[2] D. M. Cosgrove III, J. H. Petre, J. L. Waller, J. V. Roth, C. Shepherd, *et al*, "Automated control of postoperative hypertension: a prospective, randomized multicenter study," *Ann. Thorac. Surg.* Vol. 47, 678–682, 1989.

[3] S. A. Hoeksel, J. A. Blom, J. R. Jansen, J. G. Maessen, J. J. Schreuder, "Automated infusion of vasoactive and inotropic drugs to control arterial and pulmonary pressures during cardiac surgery," *Crit. Care Med.* Vol. 27, 2792–2798, 1999.

[4] G. I. Voss, P. G. Katona, H. J. Chizeck, "Adaptive multivariable drug delivery: control of arterial pressure and cardiac output in anesthetized dogs," *IEEE Trans. Biomed. Eng.* Vol. 34, 617–623, 1987.

[5] C. Yu, R. J. Roy, H. Kaufman, B. W. Bequette, "Multiple-model adaptive predictive control of mean arterial pressure and cardiac output," *IEEE Trans. Biomed. Eng.* Vol. 39, 765–778, 1992.

[6] K. Uemura, M. Sugimachi, T. Kawada, A. Kamiya, Y. Jin, *et al.*, "A novel framework of circulatory equilibrium," *Am. J. Physiol. Heart Circ. Physiol.* vol. 286, no. 6, pp. H2376–H2385, Jun. 2004.

[7] K. Uemura, T. Kawada, A. Kamiya, T. Aiba, I. Hidaka, *et al.*, "Prediction of circulatory equilibrium in response to changes in stressed blood volume," *Am. J. Physiol. Heart Circ. Physiol.* vol. 289, no. 1, H301–H307, Jul. 2005.

[8] K. Uemura, A. Kamiya, I. Hidaka, T. Kawada, S. Shimizu, *et al.*, "Automated drug delivery system to control systemic arterial pressure, cardiac output, and left heart filling pressure in acute decompensated heart failure," *J. Appl. Physiol.* vol. 100, no. 4, 1278–1286, Apr. 2006.

[9] K. L. Chien, J. A. Hrones, J. B. Reswick, "On the automatic control of generalized passive systems," *Trans. ASME.* Vol. 74, 175–185, 1952.

31st Annual International Conference of the IEEE EMBS
Minneapolis, Minnesota, USA, September 2-6, 2009

Macroscopic Two-Pump Two-Vasculature Cardiovascular Model to Support Treatment of Acute Heart Failure

Masaru Sugimachi, *Member, IEEE*, Kenji Sunagawa, *Member, IEEE*,
Kazunori Uemura, Atsunori Kamiya, Shuji Shimizu, Masashi Inagaki and Toshiaki Shishido

Abstract— **Comprehensive understanding of hemodynamics remains a challenge even for expert cardiologists, partially due to a lack of an appropriate macroscopic model. We attempted to amend three major problems of Guyton's conceptual model (unknown left atrial pressure, unilateral heart damage, blood redistribution) and developed a comprehensive macroscopic model of hemodynamics that provides quantitative information. We incorporated a third axis of left atrial pressure, resulting in a 3D coordinate system. Pump functions of left and right heart are expressed by an integrated cardiac output curve, and the capacitive function of total vasculature by a venous return surface. The equations for both the cardiac output curve and venous return surface would facilitate precise diagnosis (especially evaluation of blood volume) and choice of appropriate treatments, including application to autopilot systems.**

I. INTRODUCTION

COMPREHSNSIVE understanding of hemodynamics remains a challenge even for specialist clinicians including cardiologists. This is in part attributed to a lack of an appropriate macroscopic model of hemodynamics that would facilitate reasoning. Most cardiologists relied only on, if at all, the classical Guyton's circulatory equilibrium framework [1].

Guyton's model consists of only two subdivisions of the whole circulation: the cardiopulmonary component (in which both hearts and pulmonary vasculature are lumped) and the systemic vascular bed. These two subdivisions are characterized by the 'cardiac output curve' and 'venous return curve', respectively. The 'cardiac output curve' approximated the (total) pump function, and the 'venous return curve' approximated the capacitive function of systemic vasculature. The intersection of these curves coincides with the operating point of the circulation.

Guyton's model is, however, inappropriate (see MODEL AND METHODS) for the understanding of hemodynamics in patients with, for example, acute myocardial infarction, where only one ventricle is preferentially damaged. That is why many cardiologists gradually abandoned using Guyton's model for their reasoning.

If we can amend the shortcomings of Guyton's model and develop a more appropriate model, the new model would obviously help diagnosis procedures and treatment selection. Furthermore, the model may be able to quantify the hemodynamic abnormalities rather than just to identify them.

Therefore, the aim of this study was to develop a comprehensive macroscopic model of hemodynamics that would provide quantitative information and aid diagnosis and treatments.

II. MODEL AND METHODS

A. Shortcomings of Guyton's Model

Guyton's model has a number of problems when used in patients with unilateral heart failure.

First, the model does not provide left atrial pressure (LAP) values directly. LAP indicates the degree of pulmonary congestion and blood desaturation, and is as important as cardiac output (CO) and blood pressure.

Second, it is impossible to precisely model unilateral heart failure, which is frequently seen in patients with ischemic heart disease.

Third, in unilateral heart failure, the relative blood volumes in pulmonary and systemic vascular beds vary. As Guyton's model assumes only blood volume within the systemic vascular bed, such redistribution would shift the venous return curve even though the total blood volume remains the same.

B. Development of Comprehensive Cardiovascular Model

To solve the above problems, we extended Guyton's model.

First, a third axis of LAP was introduced in our new model (Fig. 1) [2], [3], so that LAP can be obtained directly. The pumping ability of the heart and the capacitive function of the vasculature are expressed simultaneously in the 3D space (RAP-LAP-CO coordinate system).

Second, the pumping abilities of the left and right heart are expressed separately by the respective cardiac output surfaces that are independent of each other. In an equilibrium state, by matching the cardiac output of both sides, the pumping ability of the whole heart can be integrated and expressed by a curve

Manuscript received April 7, 2009. This work was supported in part by Grant-in-Aid for Scientific Research (B 20300164, C 20500404) from the Ministry of Education, Culture, Sports, Science and Technology, by Health and Labour Sciences Research Grants (H19-nano-ippan-009, H20-katsudo -shitei-007) from the Ministry of Health Labour and Welfare of Japan.

M. Sugimachi, K. Uemura, A. Kamiya, S. Shimizu, M. Inagaki and T. Shishido are with the National Cardiovascular Center Research Institute, Suita, Osaka 5658565, Japan (corresponding author Masaru Sugimachi to provide phone: +81-6-6833-512; fax: +81-6-6835-5403; e-mail: su91mach@ri.ncvc.go.jp).

K. Sunagawa is with Kyushu University, Fukuoka 8128582 Japan. (e-mail: sunagawa@cardiol.med.kyushu-u.ac.jp).

978-1-4244-3296-7/09/$25.00 ©2009 IEEE

expressing the intersection of the two surfaces (integrated cardiac output curve, Fig. 1, thick curve).

Third, the capacitive function of total vasculature (including both systemic and pulmonary vasculatures) is expressed by the venous return surface (Fig. 1, shaded surface), which is an extension of the venous return curve. This surface expresses the changes in LAP and right atrial pressure (RAP) in response to CO change, while the total intravascular blood volume remains constant. In addition, blood redistribution between systemic and pulmonary vasculatures (without change in total blood volume) will be expressed by movement within the surface rather than by deviation from the surface.

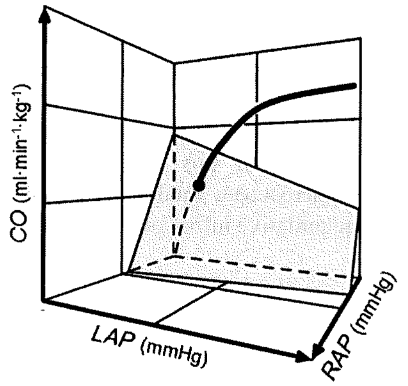

Fig. 1. An original macroscopic model of hemodynamics (an extended Guyton's model). The curve expresses the integrated pumping ability of left and right heart. The shaded surface characterizes the capacitive function of the total (systemic + pulmonary) vasculatures. The surface remains constant as long as the total intravascular blood volume remains the same. CO, cardiac output; LAP, left atrial pressure; RAP, right atrial pressure.

C. *Animal Experiments to Characterize Venous Return Surface*

Figure 2 depicts the scheme of an experiment to characterize the venous return surface. We replaced the left and right heart with roller pumps, which allows us to change CO of the right heart or left heart independently.

By adjusting the flow (i.e., CO) of the two pumps to the same level, the changes in RAP and LAP in response to a change in CO can be observed. Blood redistribution between systemic and pulmonary vasculatures can be reproduced by transiently unbalancing the flow of the two pumps.

From each dog (n = 6), we obtained 6 different sets of data (CO, RAP, LAP). These data were subjected to bivariate linear regression using RAP and LAP as independent variables and CO as the dependent variable.

III. RESULTS

Figure 3 illustrates the venous return surfaces obtained from 6 dogs. Bivariate linear regression in each animal yielded a flat surface in 3D space. The surface is shown as a line in Fig. 3, because we have projected the surface in a direction parallel to the surface. The experimental data obtained from each of the 6 animals showed good fit with the surface. In addition, the surfaces obtained from 6 animals were almost parallel, as shown by the nearly parallel 3D coordinate axes. These experimental results indicated that the venous return surface is linear and can be expressed by a common equation for all animals.

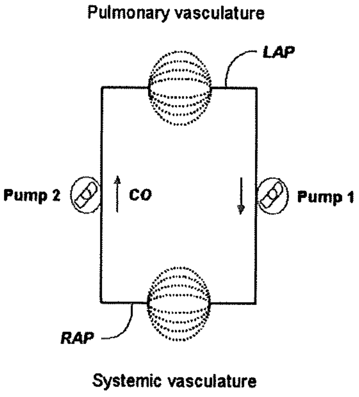

Fig. 2. An experimental scheme to characterize venous return surface. By replacing the left and right heart with roller pumps, one can change cardiac output of the right heart or left heart independently.

Further, by infusing or withdrawing known amounts of blood, we were able to derive an equation for the venous return surface as follows:

$$CO = V / 0.129 - 19.61\ RAP - 3.49\ LAP$$

where V is total intravascular stressed blood volume. This formula $[V = (CO + 19.61\ RAP + 3.49\ LAP) \times 0.129]$ can be used to quantify V from CO, RAP and LAP.

We also succeeded to quantify the integrated cardiac output curve by logarithmic functions as follows:

$$CO = S_L\ [\ln(LAP-2.03)+0.80]$$

$$CO = S_R\ [\ln(RAP-2.13)+1.90]$$

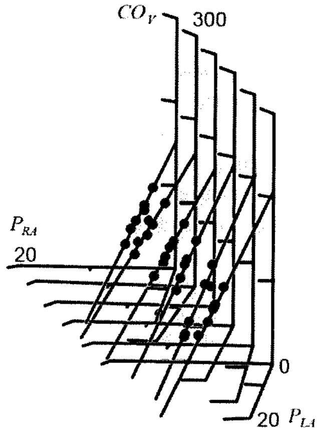

Fig. 3. Superimposed venous return surfaces obtained from 6 dogs. For each dog, the venous return surface (RAP-LAP-CO relationship) in 3D coordinate system was projected in a direction parallel to the surface, and was superimposed with each other.

where S_L and S_R are parameters expressing the pumping ability of the left and right heart, respectively. These equations are also useful for quantifying the pumping ability of right and left heart (S_L = CO / [ln(LAP - 2.03) + 0.80], S_R = CO / [ln(RAP - 2.13) + 1.90]).

Using this model, we are able to predict with acceptable precision the hemodynamics after infusion or withdrawal of known amounts of blood (CO: $y = 0.93x + 6.5$, $r^2 = 0.96$, SEE = 7.5 ml·min^{-1}·kg^{-1}; LAP: $y = 0.90x + 0.5$, $r^2 = 0.93$, SEE = 1.4 mmHg; RAP: $y = 0.87x + 0.4$, $r^2 = 0.91$, SEE = 0.4 mmHg) (Fig. 4) [3].

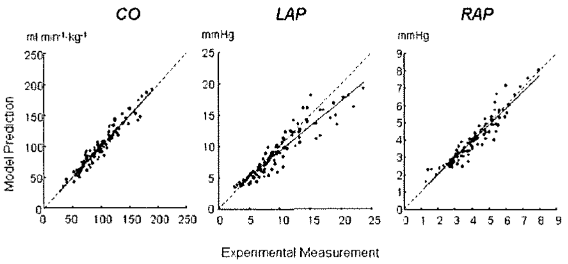

Fig. 4. Prediction of CO, LAP, and RAP based on our comprehensive macroscopic model of hemodynamics.

IV. DISCUSSION

A. Difficulty in Decision Making of Heart Failure Treatment

Three hemodynamic variables: blood pressure, CO and LAP, appear to be the most essential factors influencing the survival of patients with heart failure. Our model clearly indicates that pump functions of left and right heart and total intravascular blood volume are determinants of CO and LAP. Systemic vascular resistance is an additional determinant of blood pressure.

For clinicians, the evaluation of blood volume is relatively difficult compared to pump functions and vascular resistance. In practice, clinicians have been using RAP as a proxy for blood volume. It is clear from our results [V = (CO + 19.61 RAP + 3.49 LAP) × 0.129] that blood volume (V) is not solely determined by RAP. Rather, all three parameters of CO, RAP and LAP are necessary to evaluate blood volume. The equation indicates that an increase of RAP by 1 mmHg is equivalent to an LAP increase of 5.6 mmHg, and a CO increase of 19.61 mL/min/kg (ca. 0.98 L/min for a 50-kg patient).

B. Application of the Model: Autopilot System

The biggest benefit of our comprehensive visual model of hemodynamics is that it enables us to diagnose the abnormality of cardiovascular system in a quantitative manner. This would lead to appropriate selection of drugs and their doses.

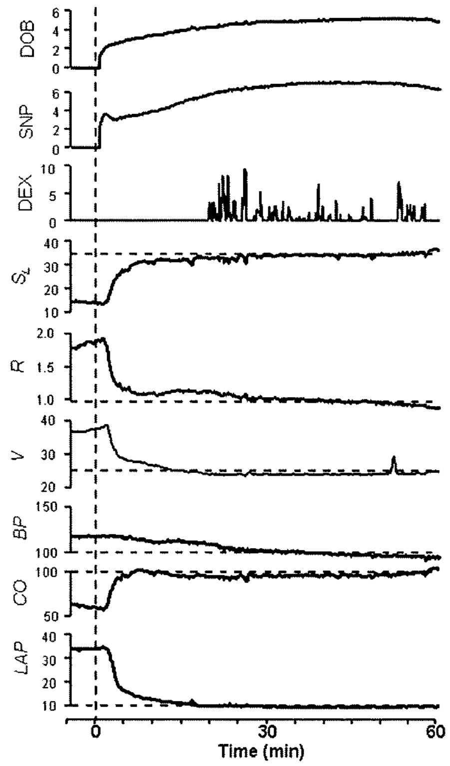

Fig. 5. An example of correction of hemodynamics with an autopilot system. By normalizing cardiovascular properties [pump function (S_L), resistance (R), blood volume (V)] with the administration of dobutamine (DOB), sodium nitroprusside (SNP), and dextran 40 solution (DEX), all the abnormal hemodynamic variables (increased blood pressure [BP], decreased cardiac output [CO], and elevated left atrial pressure [LAP]) were resolved rapidly, sufficiently, and stably.

As shown in Fig. 5, by translating hemodynamic variables into cardiovascular properties (pump function, vascular resistance, and blood volume), and by controlling each of these parameters with individual drug with preferential effect on the parameter, we are able to correct automatically all the parameters of blood pressure, CO and LAP rapidly, stably, and simultaneously.

Using an autopilot system to administer dobutamine (DOB at 5 ± 3 mg·kg^{-1}·min^{-1}), nitroprusside (SNP at 4 ± 2 mg·kg^{-1}·min^{-1}), dextran infusion (DEX at 2 ± 2 ml·kg^{-1}), and furosemide (10 mg in one, 20 mg in one) in 12 dogs with acute heart failure rapidly normalized blood pressure, CO, and LAP in 5 ± 7, 7 ± 5, and 12 ± 10 minutes, respectively. The normalized values remained stable thereafter (RMS values, blood pressure = 4 ± 3 mmHg, CO = 5 ± 2 ml·min^{-1}·kg^{-1}, LAP = 0.8 ± 0.6 mmHg).

V. CONCLUSION

We have successfully developed a comprehensive macroscopic model of hemodynamics that provides quantitative information. Using a 3D coordinate system, the pump functions of left and right heart are expressed by an integrated cardiac output curve, and the capacitive function of total vasculature by a venous return surface. The equations of both the cardiac output curve and venous return surface would facilitate accurate diagnosis (especially evaluation of blood volume) and choice of appropriate treatments, including application to autopilot systems.

REFERENCES

[1] A. C. Guyton, "Determination of cardiac output by equating venous return curves with cardiac response curves," *Physiol. Rev.* vol. 35, no. 1,123–129, Jan. 1955.

[2] K. Uemura, M. Sugimachi, T. Kawada, A. Kamiya, Y. Jin, *et al.*, "A novel framework of circulatory equilibrium," *Am. J. Physiol. Heart Circ. Physiol.* vol. 286, no. 6, pp. H2376–H2385, Jun. 2004.

[3] K. Uemura, T. Kawada, A. Kamiya, T. Aiba, I. Hidaka, *et al.*, "Prediction of circulatory equilibrium in response to changes in stressed blood volume," *Am. J. Physiol. Heart Circ. Physiol.* vol. 289, no. 1, H301–H307, Jul. 2005.

J Physiol Sci
DOI 10.1007/s12576-010-0086-y

ORIGINAL PAPER

Right ventricular stiffness constant as a predictor of postoperative hemodynamics in patients with hypoplastic right ventricle: a theoretical analysis

Shuji Shimizu · Toshiaki Shishido · Dai Une · Atsunori Kamiya · Toru Kawada · Shunji Sano · Masaru Sugimachi

Received: 9 December 2009 / Accepted: 10 January 2010

Abstract One and a half ventricle repair (1.5VR) is a surgical option for hypoplastic right ventricle (RV). The benefits of this procedure compared to biventricular repair (2VR) or Fontan operation remain unsettled. To compare postoperative hemodynamics, we performed a theoretical analysis using a computational model based on lumped-parameter state-variable equations. We varied the RV stiffness constant (B_{RV}) to simulate the various RV hypoplasia, and estimated hemodynamics for a given B_{RV}. With $B_{\mathrm{RV}} < 150\%$ of normal, cardiac output was the largest in 2VR. With $B_{\mathrm{RV}} > 150\%$, cardiac output became larger in 1.5VR than in 2VR. With $B_{\mathrm{RV}} > 250\%$, RV end-diastolic volume was almost the same between 1.5VR and 2VR, and a rapid increase in atrial pressure precluded the use of 1.5VR. These results indicate that the beneficial effect of 1.5VR depends on the RV stiffness constant. Determination of management strategy should not only be based on the morphologic parameters but also on the physiological properties of RV.

Keywords One and a half ventricle repair · Right ventricular stiffness · Hypoplastic right ventricle · Computational model

Introduction

One and a half ventricle repair (1.5VR) is a surgical option for hypoplastic right ventricle (RV) caused by various congenital heart diseases including pulmonary atresia with intact ventricular septum (PA/IVS), Ebstein's anomaly or their relatives. In this procedure, the superior vena cava (SVC) is directly connected to the pulmonary artery (PA). Therefore, the blood from SVC directly enters PA, whereas the blood from the inferior vena cava (IVC) is pumped by RV to PA. This procedure is clinically acceptable because of its low surgical risk [1, 2]. However, the benefits of this procedure on postoperative hemodynamics in patients with a wide spectrum of RV hypoplasia compared to other procedures such as biventricular repair (2VR) and Fontan operation remain unsettled [3]. Furthermore, conversion to Fontan circulation was required late after 1.5VR in a possibly inappropriate candidate [4].

Although various authors reported an arbitrary selection scheme for the procedures based on RV morphology such as RV end-diastolic volume (RVEDV) [1, 2, 5], the long-term outcomes of 1.5VR have remained insufficiently known [5]. The previous criteria do not likely predict postoperative hemodynamics of these complex circulations accurately because morphological values measured preoperatively largely depend on the RV preload and afterload conditions, which change remarkably between subjects and between before and after the operation.

Hypoplastic RV is physiologically characterized by increased RV stiffness, caused by hypertrophy and

---

S. Shimizu (✉) · T. Shishido · D. Une · A. Kamiya · T. Kawada · M. Sugimachi
Department of Cardiovascular Dynamics, Advanced Medical Engineering Center, National Cardiovascular Center Research Institute, 5-7-1 Fujishiro-dai, Suita, Osaka 565-8565, Japan
e-mail: shujismz@ri.ncvc.go.jp

S. Shimizu · S. Sano
Department of Cardiovascular Surgery, Okayama University Graduate School of Medicine, Dentistry and Pharmaceutical Sciences, Okayama, Japan

S. Shimizu
Japan Association for the Advancement of Medical Equipment, Tokyo, Japan